Proceedings of the 21st ICSMGE, Vienna, Austria, 14 – 19 June 2026. Pistrol, Adam & Schweiger (eds.)
Published by: ÖGG, Austrian Society for Geomechanics, Salzburg, Austria, ISBN 978-3-9503898-4-5
https://doi.org/10.53243/ICSMGE2026-1387

Numerical simulation of dynamic soil compaction with an oscillatory roller to investigate improvement depth and measurement depth

Ivan Paulmichl, Ralph Bergman, Christoph Adam
Universität Innsbruck, Unit of Applied Mechanics, Austria, ivan.paulmichl@uibk.ac.at

ABSTRACT: The presented study investigates the improvement depth and measurement depth of an oscillatory roller using numerical models of the roller-subsoil interaction system. Firstly, the dynamic response of the drum oscillating in a predefined "settlement through" on a layered linear elastic half-space is predicted based on plane-strain finite element (FE) simulations. By varying thickness and stiffness of the layer, different assumed compaction states are modeled and their influence on the drum response is studied in terms of accelerations in the time and frequency domain. Additionally, an analysis is conducted on a compaction indicator that was developed for the first operational, work-integrated, continuous compaction control (CCC) system for oscillatory rollers. By comparing the dynamic response for different layered half-spaces, an estimation for the measurement depth is derived. Secondly, a plane-strain FE model of a moving roller is presented. This model captures the nonlinear, inelastic and cyclic soil behavior by using the intergranular enhanced hypoplastic constitutive law. It simultaneously predicts the compaction process and the dynamic drum response within the framework of CCC. The effect of a roller pass at standard excitation frequency on an initially very loose to dense homogeneous subsoil is explored in terms of void ratio reduction, aiming to predict the improvement depth of a specific oscillatory roller. The assessment of measurement depth entails the implementation of a localized loose soil zone placed within both hypoplastic and linear elastic subsoils. This "weak spot" is investigated further through an examination of its influence on the drum response, measured by the CCC parameter, as it is increased in depth. The findings indicate that the proposed models effectively predict both improvement and measurement depth and qualitatively reproduce the response characteristics of the interacting oscillatory roller-subsoil system observed in field tests.

KEYWORDS: Oscillatory roller, dynamic soil compaction, roller-integrated compaction control, finite element modeling.

1 INTRODUCTION

Over the past seven decades, earthworks compaction has been revolutionized, largely driven by the advent of innovative roller-based soil compaction/stiffness measurement systems based on the dynamic excitation of the drum (Paulmichl et al., 2025). The interaction between the dynamically excited drum and the soil or fill material to be compacted forms the basis for work-integrated, continuous compaction control (CCC). Combined with positioning (GPS) and on-board computing, CCC enables real-time quality control and provides more comprehensive quality assurance data than spot tests.

Numerous aspects of vibrating roller-subsoil interaction system and vibrating roller-measured soil compaction/stiffness (including compaction depth and measurement depth) have been comprehensively investigated both experimentally and numerically (e.g. Adam, 1996; Anderegg and Kaufmann, 2004; Kopf and Erdmann, 2005; Rinehart and Mooney, 2009; Erdmann and Adam, 2014; Erdmann, 2018; Fathi et al., 2021; Hager, 2022). In contrast, there are very few publications investigating soil compaction with oscillatory rollers (e.g. Kopf, 1999; Pistrol, 2016; Erdmann, 2018; Paulmichl, 2019). To the authors' knowledge, Kopf (1999) and Pistrol (2016) are the only researchers who have conducted experimental assessments of measurement depth using oscillatory rollers. The oscillating drum of a HAMM HD+ 90 VO tandem roller with standard operating parameters (excitation frequency: 39 Hz; roller speed: 4 km/h) clearly detected mattresses buried in sandy gravel at depths of 0.15 m and 0.55 m via a decrease in the CCC value (Pistrol and Adam, 2018). Based on the finite element (FE) models developed by Paulmichl (2019), first approaches to the numerical estimation of the measurement depth of the CCC value for oscillatory rollers patented ten years ago (Pistrol et al., 2016) are provided in a recent master's thesis (Bergman, 2025) and a recently published paper (Paulmichl et al., 2025).

In the light of this, this paper presents numerical modeling approaches to assess both improvement depth and measurement depth reflected in the roller-measured CCC value of one oscillatory roller (HAMM HD+ 90 VO). In a first approach, a fully compacted soil and a stationary roller are assumed. FE simulations of a drum oscillating on stratigraphies of soft over stiffer linear elastic soil are performed to examine the measurement depth of the patented CCC value. For this analysis, a circular contact surface between the drum and the soil is prescribed (based on Paulmichl, 2019). A second approach analyzes the compaction effect of a roller passing over a hypoplastic subsoil, as well as the motion of the drum. The depth to which an inhomogeneity is reflected in the CCC value is determined by modeling a local heterogeneity with variable depth.

2 MODELLING APPROACH 1

2.1 *Finite element simulation*

The plain strain FE model of a stationary oscillating drum of a HAMM HD+ 90 VO tandem roller, which was proposed by Paulmichl (2019) and extended by Bergman (2025), is used to assess the dynamic behavior of the drum under given compaction conditions. To this end, the soil stiffness is defined a priori in terms of *Young*'s modulus E, and the contact zone between the drum and soil is modeled as a circular curve (so called "settlement trough" according to Paulmichl et al., 2019).

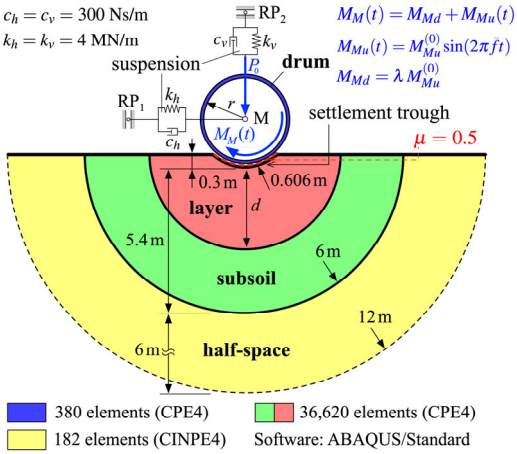

Figure 1. Finite element model 1 (schematic): stationary oscillatory roller.

Figure 1 shows the used 2D FE model (out-of-plane thickness: 1.68 m). The steel drum (radius: $r = 0.6$ m; width $b = 1.68$ m; mass $m = 1{,}851$ kg; mass moment of inertia: $I = 412$ kg m^2) oscillates in a prescribed settlement trough with a radius $R = 1.01\ r$ (Paulmichl et al., 2025) on a layered half-space (soft layer over stiffer subsoil). The horizontal and vertical spring-damper elements attached to the drum center (node M) represent the viscoelastic connection to the roller frame (spring coefficients: k_h and k_v; damping parameters: c_h and c_v). The contact between the drum and the soil is described by dry friction according to *Coulomb*'s law with constant coefficient of friction $\mu = 0.5$. Increasing the thickness d of the layer from 0 to 5.4 m models stratigraphies of a soft layer ($E_L = 16$ MN/m^2) over a stiffer subsoil ($E_S = 32$ MN/m^2). The thickness d at which the underlaying subsoil is no longer reflected in the dynamic drum response (in terms of the CCC value according to Pistrol, 2016) is defined as the "measurement depth" d_{CCC}.

The steps of the numerical analysis performed with ABAQUS/Standard (Dassault Systèmes SIMULIA, 2015) are as follows: After the geostatic step (step 1), contact between the drum and soil is established by applying a vertical displacement at the nodes RP and M (step 2). Step 3 involves loading of the drum by applying the static axle load P_0 of 44,130 N to node M. The displacement applied in step 2 is determined iteratively with the condition that the slope of the drum displacement at the end of step 3 is zero. This is essential for reliable results (Bergman, 2025). Finally, in step 4, an oscillation moment $M_{Mu}(t)$ is applied to node M, thereby exciting the statically loaded drum harmonically. For the roller under consideration, the amplitude $M_{Mu}^{(0)}$ of the sinusoidal torque $M_{Mu}(t)$ at the standard excitation frequency $\bar{f}$ of 39 Hz is 54,947 Nm (Paulmichl et al., 2019). The resulting amplitude of the tangential displacement at the edge of a lifted drum is 1.44 mm (Pistrol, 2016). In a further investigation, a constant driving torque M_{Md} is considered as well. M_{Md} is assumed to be 5% of $M_{Mu}^{(0)}$ (i.e., $\lambda = 0.05$ according to Figure 1), analogous to Paulmichl et al. (2019). M_{Md} is applied in step 3 prior to the dynamic step 4.

The layer, subsoil, and half-space are modeled with a density ρ of 2000 kg/m^3 and a *Poisson*'s ratio ν of 0.3. The half-space is assigned the modulus E of the adjacent soil. Material damping is considered in terms of *Rayleigh* damping. The parameters α and β are set to 28.6 and 0.0000952, respectively, providing a damping of about 5% at the frequency $f = \bar{f}$. The maximum time increment was set to $0.005/\bar{f}$.

2.2 *Drum response*

First, the dynamic drum response for the model without driving torque ($\lambda = 0$) is discussed. Figure 2(a) shows the horizontal acceleration of the drum center M for three excitation periods and four layer thicknesses. The horizontal response is symmetric with respect to the time axis and periodic, with a period equal to the excitation period. The amplitude remains nearly unaffected by the change in layer thickness, with values around 14 m/s^2 in all four cases. The curves can be interpreted as a sinusoidal signal, whose peaks are cut off. A kink indicates the transition from the stick phase to the slip phase, and vice versa (Paulmichl et al., 2019). During the slip phase, the horizontal acceleration component decreases. A change in layer thickness slightly affects the shape of the horizontal acceleration response.

Due to the geometry of the prescribed settlement trough, the period of the vertical acceleration response is one half of the excitation period (see Figure 2(b)). Clear differences are observed for different layer thicknesses. For a layer thickness of 0 (i.e., a homogeneous soil with $E = 32$ MN/m^2), the response is asymmetric and two peaks are observed in the positive part of the response for each period (see Figure 2(b), black line). As the layer thickness increases, the two "peaks" flatten out, and the vertical response becomes more symmetrical.

Plotting the vertical acceleration component against its horizontal counterpart, results in a meaningful response representation, as shown in Figure 2(c) for the 35th oscillation cycle. The area enclosed by this curve corresponds to the CCC value of oscillatory rollers developed by Pistrol (2016). As can be seen, the area, and thus, the CCC value, for the four layer thicknesses differ significantly. This change is primarily caused by the difference in vertical accelerations.

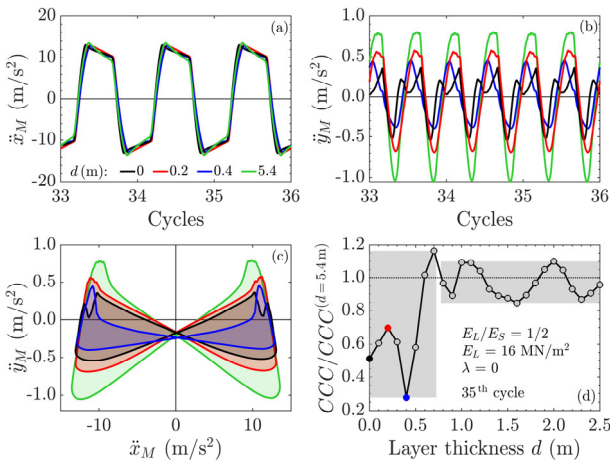

Figure 2. (a) Horizontal and (b) vertical drum center acceleration over three oscillation cycles, (c) superposition figures for four layer thicknesses d, (d) normalized CCC value depending on d ($\lambda = 0$).

Figure 2(d) illustrates how the CCC value changes with layer thickness d during the 35th excitation period. The CCC value is normalized by the CCC value of the model with 5.4 m layer thickness. This value, $CCC^{(d = 5.4\ m)}$, is used as a reference, because it is assumed that changes in soil stiffness at this depth do not affect the dynamic drum response. Up to a layer thickness of 0.7 m, the CCC value varies by approximately 90%, as indicated by the gray rectangle on the left side of the figure. From a layer thickness of 0.8 m onwards, the CCC value differs by only about 10% from the reference value $CCC^{(d = 5.4\ m)}$, as indicated by the right gray rectangle in the figure. Based on this sudden decrease in the range of variation of the CCC value, an estimated measurement depth d_{CCC} of approximately 0.8 m can be determined. The remaining differences between the CCC value and the reference value are assumed to be due to the "sensitivity" of the numerical model. Details on the discussion of the sensitivity of the numerically predicted drum response can be found in Bergman (2025).

Figure 3(a) and Figure 3(b) show the horizontal and vertical drum responses in the frequency domain. Values that are practically zero, except for integer multiples of the excitation periods, are omitted for clarity. Figure 3(a), representing the horizontal drum acceleration, contains only odd harmonics because the "peak cut" of the response due to the slip phases is symmetrical. Overtones at uneven multiples of the excitation frequency indicate that the drum motion includes slip phases. The largest amplitudes belong to the operating frequency and are practically identical for the different layer thicknesses. In contrast, the frequency content of the vertical response in Figure 3(b) contains only even harmonics. The amplitudes at $f/\bar{f} = 2$, however, are strongly influenced by the subsoil and vary, for instance, between 0.25 m/s^2 ($d = 0$) and 0.91 m/s^2 ($d = 5.4$ m) for the four selected layer thicknesses.

Figure 3(c) shows the representation of the amplitude of the first harmonic of the horizontal response, normalized to the corresponding amplitude of the model with $d = 5.4$ m, as a function of layer thickness d. This figure illustrates the minor influence of the subsoil over the entire range of d. The variation in normalized amplitudes is a maximum of approximately 5%. A glance at the evaluation of the vertical response at $f/\bar{f} = 2$, shown in Figure 3(d), reveals that the fluctuation range is approximately 100% up to $d = 0.7$ m and only about 23% from $d = 0.8$ m onwards. Therefore, the estimated measurement depth is $d_{CCC} = 0.8$ m. The curves in Figure 2(d) and Figure 3(d) are practically identical in terms of quality, and the same measurement depth can be derived from both.

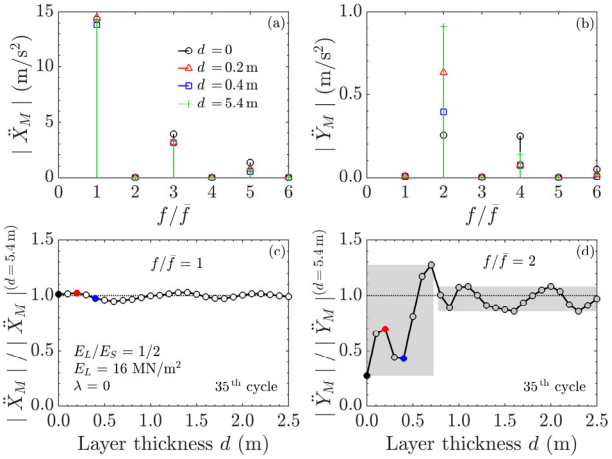

Figure 3. Amplitude spectrum of the (a) horizontal and (b) vertical drum center acceleration for four layer thicknesses d, (c) normalized first harmonic of the horizontal acceleration, and (d) normalized second harmonic of the vertical acceleration as a function of d ($\lambda = 0$).

Applying a driving torque to the drum ($\lambda = 0.05$) results in an asymmetric horizontal acceleration response (see Figure 4(a)), which leads to asymmetric and rotated superposition figures (see Figure 4(c)). Thus, the frequency spectrum contains both odd and even harmonics (see Figure 5(a)). The amplitudes of the harmonics are again only slightly influenced by the subsoil, for example, the amplitudes of the first harmonic range from about 13.4 m/s^2 to 13.9 m/s^2. Figure 4(b) shows that the vertical drum response is also now dominated by the excitation frequency. The corresponding frequency spectrum also contains both odd and even harmonics that depend strongly on the subsoil stiffness (see Figure 5(b)).

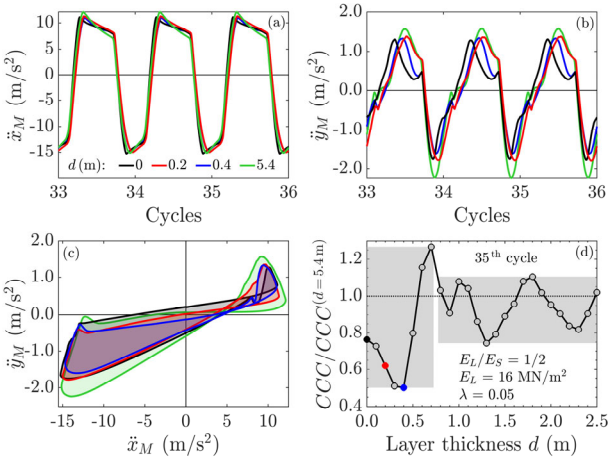

Figure 4. (a) Horizontal and (b) vertical drum center acceleration over three oscillation cycles, (c) superposition figures for four layer thicknesses d, (d) normalized CCC value in dependence of d ($\lambda = 0.05$).

Consequently, the normalized CCC value for the 35th oscillation cycle fluctuates considerably up to a layer thickness of 0.7 m (see Figure 4(d)). Once again, a decrease in fluctuations from approximately 107% to 35% is observed at a layer thickness of 0.8 m. Thus, the range of variation from $d = 0.8$ m onwards is slightly greater than in the model without driving torque (compare Figure 4(d) and Figure 2(d)). Nevertheless, a clear drop in the fluctuation rate of the CCC value is observed from $d = 0.8$ m onwards. Thus, d_{CCC} is estimated at 0.8 m.

The observed variation in CCC values is again mainly influenced by fluctuations in vertical responses (compare Figure 4(d) with Figure 5(c) and Figure 5(d)).

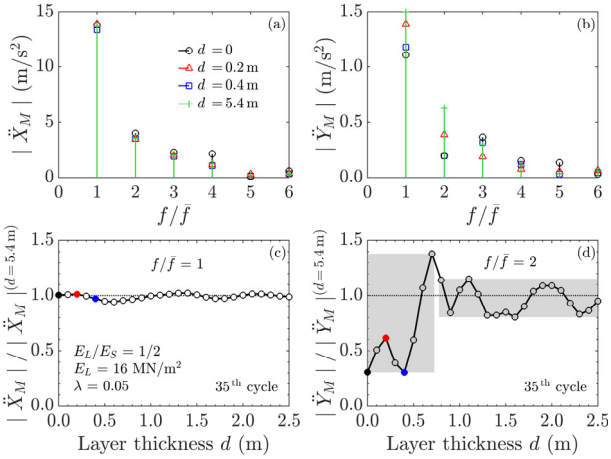

Figure 5. Amplitude spectrum of the (a) horizontal and (b) vertical drum center acceleration for four layer thicknesses d, (c) normalized first harmonic of the horizontal acceleration, and (d) normalized second harmonic of the vertical acceleration as a function of d ($\lambda = 0.05$).

3 MODELLING APPROACH 2

3.1 *Finite element simulation*

According to Paulmichl et al. (2020, 2025), soil compaction due to cyclic shearing caused by an oscillatory roller can be simulated using the basic hypoplastic constitutive model from von Wolffersdorff (1996), enhanced by the intergranular strain concept after Niemunis and Herle (1997). Table 1 specifies for Hochstetten sand the parameters required to describe a granular soil using this constitutive model: eight hypoplastic (green), five intergranular strain (orange), und three linear elastic parameters (grey).

Table 1. Hochstetten sand: hypoplastic (Niemunis and Herle, 1997; Herle, 1997) and linear elastic parameter set.

φ_c (°)	h_s (MN/m^2)	n	e_{d0}	e_{c0}	e_{i0}	α	β
33	1,500	0.28	0.55	0.95	1.05	0.25	1.50
R	m_R	m_T	β_r	χ	E (MN/m^2)	c (kN/m^2)	ν
10^{-4}	5	2	0.5	6	10	5	0.48

To simulate the compaction effect of a moving oscillatory roller (HAMM HD+ 90 VO, as described in section 2) and calculate the CCC value based on the motion of the drum (as described in section 2.2), the two-dimensional FE model proposed and verified by Paulmichl et al. (2020) has been further developed. The more advanced model is shown schematically in Figure 6 ("model 2"). The suspension of the drum was implemented as described in modeling strategy 1 ($k_h = k_v$, $c_h = c_v$; see Figure 1 for values). Additionally, model 2 without the vertical spring-damper element ("model 2-LC") was considered as a limit case to prevent possible loss of contact between the drum and soil.

The "protective foil" applied to the soil surface (Paulmichl et al., 2020) to ensure the numerical stability in ABAQUS/Standard simulations, together with the UMAT according to Mašín (2017), is no longer necessary when using the in-house UMAT (Wolf, 2022).

The roller speed v_0 was defined as a boundary condition in the reference points RP (see Figure 6). This was achieved by creating another simulation step (in addition to the steps described in section 2.1) to accelerate the drum to speed v_0 before the harmonic moment $M_{Mu}(t)$ was applied. The same maximum time increment as in model 1 was used.

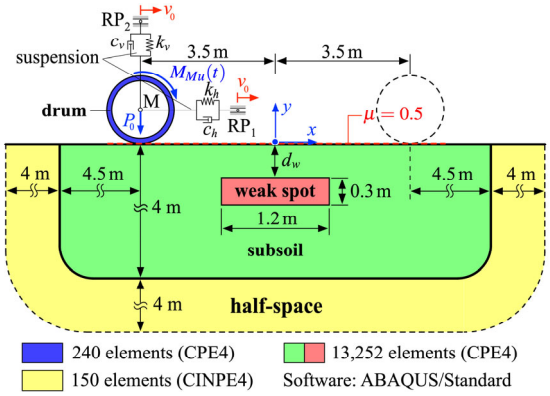

Figure 6. Finite element model 2 (schematic): moving oscillatory roller.

3.2 *Compaction by shearing*

The cyclic behavior of the hypoplastic constitutive model used is examined by simulating the shearing of a single element. To this end, the hypoplastic constitutive model was implemented in the Incremental Driver (Niemunis, 2023) as a user-defined material using the in-house UMAT (Wolf, 2022).

Figure 7 shows an exemplary case of the development of the void ratio e due to shearing with a shear strain amplitude of 5% and a vertical stress of 25 kN/m^2, assuming an initially very loose soil ($e_0 = 0.92$). Starting from the third cycle, loosening (increase in void ratio) and compaction (reduction in void ratio) alternate. The void ratio at the end of one cycle is smaller than at the beginning, indicating permanent compaction. However, this increase in compaction decreases significantly with each cycle and becomes barely noticeable from the 12th cycle onwards. Ultimately, a "maximum" compaction state is reached and the "fly-like" curves are nearly on top of each other. Depending on the shear strain amplitude and the initial void ratio, loosening rather than compaction is predicted, especially at low vertical stresses. Paulmichl et al. (2025) have shown that decreasing the void ratio increases the soil stiffness. Therefore, the constitutive model used can basically represent the increase in stiffness due to "compaction by shearing".

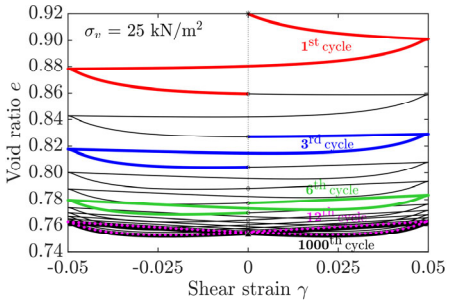

Figure 7. Void ratio e as a function of the shear strain.

3.3 *Compaction effect in terms of void ratio reduction*

The compaction effect was numerically simulated assuming a homogeneous subsoil with an initial void ratio e_0 for a pass with a HAMM HD+ 90 VO roller at standard operation parameters (excitation frequency: 39 Hz; roller speed: 4 km/h). To map the range from very loose to dense, four values were assumed for the initial void ratio e_0 as follows: 0.92 (very loose), 0.85 (loose), 0.75 (medium dense) and 0.65 (dense).

Figure 8 shows the predicted void ratio e with respect to the horizontal distance x_M of the drum center from the observation point in the middle of the model ($x = 0$) at a depth of $y = -0.09$ m. The aforementioned alternating phases of loosening and compaction can be seen as small oscillations in the curves based on model 2 (solid lines). For an initially very loose soil, the void ratio decreases continuously as the roller approaches. Approximately half of the reduction in void ratio takes place after the roller has passed the observation point. If the soil is initially loose to dense, the void ratio also decreases at first. Subsequently, however, the void ratio increases as result of the bow wave developing at the surface, with the resulting loosening being approximately maximum when the drum center is located above the observation point ($x_M = 0$). This is followed by continuous compaction, with the amount of the permanent compaction increasing as the initial void ratio decreases. At the depth under consideration, the void ratio is significantly influenced in the range of approximately $x_M = -0.5$ m to $x_M = 0.4$ m ($e_0 = 0.92$) and $x_M = -0.8$ m to $x_M = 0.7$ m ($e_0 = 0.65$), respectively. That is, the reach of the oscillatory roller is at least 1 to 1.5 times the drum radius. Model 2-LC yields qualitatively comparable results (dotted lines in Figure 8). Quantitatively, however, differences are apparent, particularly regarding the evolution of the void ratio in the range $x_M < 0$ and for loose to dense subsoils.

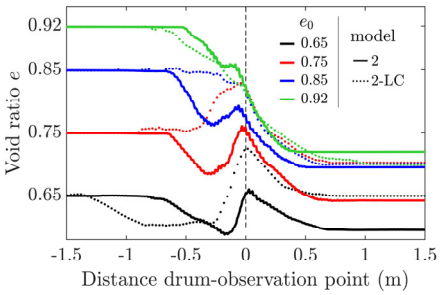

Figure 8. Evolution of void ratio at $x = 0$ and $y = -0.09$ m as a function of the distance from the drum (x_M) to the observation point (x).

The computed void ratio e was evaluated over the depth at 5 cm intervals horizontal distance and averaged over a 1 m distance (-0.5 m $\leq x \leq 0.5$ m). Figure 9(a) shows the corresponding depth profiles. The change in void ratio e_0–e is related to e_0. The void ratio changes numerically down to a depth of around 0.8 m (model 2) to 1.1 m (model 2-LC). The maximum reduction in the initial void ratio is predicted by model 2 to be approximately 11% ($e_0 = 0.65$) to 21% ($e_0 = 0.92$) at a depth of around 0.09 m ($e_0 = 0.92$) to 0.22 m ($e_0 = 0.65$). This depth is defined as the "improvement depth" d_e. Model 2-LC, by contrast, predicts lower compaction for loose to dense subsoils, as well as a pronounced near-surface loosening for very dense soils. Moreover, it yields an improvement depth of 0.2 m to 0.4 m, approximately twice that of model 2, primarily due to the absence of the restoring vertical spring force.

The influence of the roller speed v_0 on the predicted change in void ratio e of an initially very loose soil is discussed next. Two additional roller speeds v_0 are considered: one below the default value $v_0 = 4$ km/h (3 km/h) and one above it (5 km/h). Figure 9(b) illustrates the results in terms of the normalized change in void ratio. At first glance, it can be clearly seen that the roller speed considerably affects the compaction effect of the oscillating drum. The predicted maximum reduction in e_0 ranges from approximately 17% ($v_0 = 5$ km/h) to 26%

(v_0 = 3 km/h) at a depth of around 0.09 m (model 2), and from 16% (v_0 = 5 km/h) to 28% (v_0 = 3 km/h) at a depth of around 0.1 m to 0.22 m (model 2-LC), respectively. Thus, both models predict a significant increase in compaction as the roller speed decreases, while the improvement depth remains virtually unaffected (except for model 2-LC at v_0 = 3 km/h). However, the depth of influence increases somewhat more significantly as the roller speed decreases.

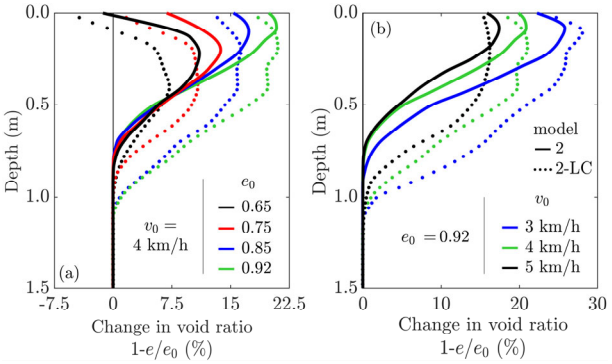

Figure 9. Depth profiles of the predicted change in void ratio: variation of (a) the initial void ratio e_0 and (b) the roller speed v_0.

3.4 *Drum response*

To gain a deeper insight into the drum response characteristics, the computed drum accelerations assuming a homogeneous subsoil are transformed into the frequency domain after the removal of the frequency tones below the excitation frequency $\bar{f}$ and above $5\bar{f}$. The resulting frequency response is plotted against the ratio of the frequency f to $\bar{f}$. Figure 10 shows that the frequency spectra contain both odd and even harmonics, but they are dominated by the excitation frequency. The additional harmonics in the horizontal drum acceleration spectra (see Figure 10(a)) can be traced back to the asymmetrical "peak cut" in the slip phases of the drum motion. The drum operates on the slope of the settlement trough, and thus, the vertical acceleration spectra are dominated by the excitation frequency (see Figure 10(b)). As e_0 decreases, the amplitude of the first harmonic in the horizontal acceleration spectra increases from 2.6 to 4.6 m/s^2. The amplitude of the second harmonic in the vertical acceleration spectra also increases from approximately 0.2 to 0.6 m/s^2, i.e., 31% and 82% of the amplitude of the first harmonic, which remains virtually unaffected. In contrast, model 2-LC predicts a decrease in amplitude of both the first harmonic in the horizontal and vertical acceleration spectra.

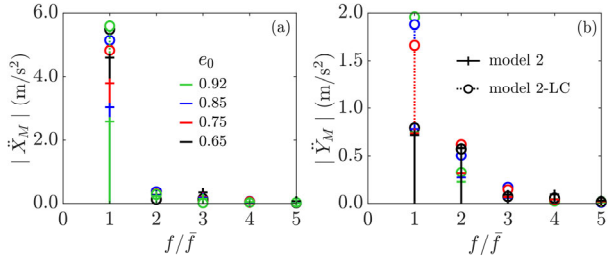

Figure 10. Amplitude spectrum of the (a) horizontal and (b) vertical acceleration of the drum center.

To validate the numerically predicted drum response with experimental data, the frequency spectra for e_0 = 0.75, as shown in Figure 10, are normalized to a maximum value of one. Figure 11 compares these spectra (in blue and green) with the amplitude spectra of the drum acceleration recorded during the 11th pass on sandy gravel (red), using the same roller as assumed in the presented simulations (Pistrol, 2016). As can be seen, the overtones in the measured data are also present in the numerically simulated data. Moreover, the corresponding normalized amplitudes up to the second harmonics are of the same magnitude. The only exceptions are the amplitudes of the third harmonics, which are underestimated in the simulations in both the horizontal and vertical amplitude spectra.

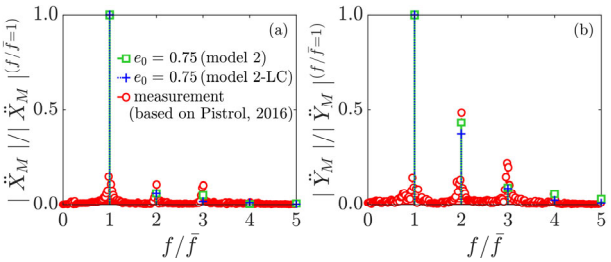

Figure 11. Normalized amplitude spectrum of the (a) horizontal and (b) vertical accelerations of the drum center: simulation vs. measurement.

Finally, the influence of a "weak spot" on the drum response is examined using the CCC value. To this end, additional numerical simulations were performed considering a local inhomogeneity (see Figure 6). This inhomogeneity is modeled as hypoplastic, assuming that it is initially very loose ($e_0^{(w)}$ = 0.92) and dense ($e_0^{(w)}$ = 0.65). To model fully compacted surrounding subsoil, both the extended hypoplastic model (e_0 = 0.56, "model 2-A") and the linear elastic model (E = 16 MN/m^2, "model 2-B") are used. The depth d_w of the weak spot was varied up to 1.2 m in increments of 0.3 m. The CCC value was evaluated for each oscillation cycle during a complete roller pass. The mean value (average of five consecutive cycles according to Pistrol (2016)) is plotted in Figure 12 over the distance x traveled between -2.5 m and 2.5 m. The gray shading indicates the location of the weak spot.

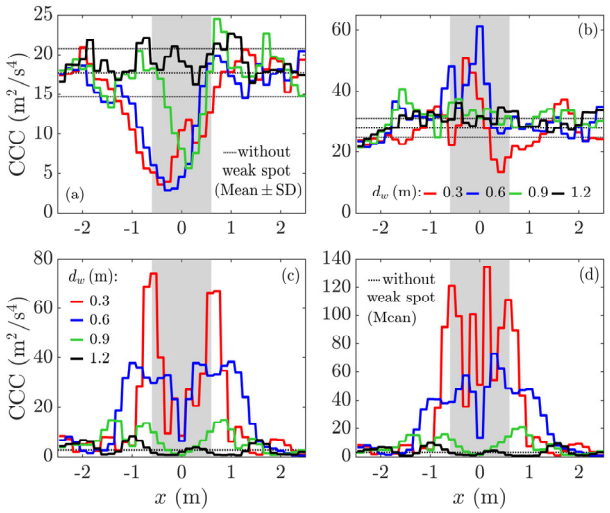

Figure 12. Evolution of the CCC value for different depths d_w of the weak spot (gray shaded area): (a) model 2-A and (b) model 2-LC-A ($e_0^{(w)}$ = 0.65); (c) model 2-B and (d) model 2-LC-B ($e_0^{(w)}$ = 0.92).

As shown in Figure 12(a), weak spots up to depths of d_w = 0.9 m result in a significant decrease in the CCC value below the mean value based on the homogeneous model (dotted line) and are, thus, clearly reflected in the drum response (model 2-A). At depths greater than 1.2 m, the standard deviation of the predicted CCC value is similar to that of the homogeneous case (thin dotted lines).

For model 2-LC-A at a depth of d_w = 0.3 m, the CCC value increases significantly in the vicinity of the weak spot before dropping noticeably below its initial value (see Figure 12(b)). At d_w = 0.6 m, the increase begins slightly before the inhomogeneity. After that, it drops back down to the initial

level. At depths greater than $d_w = 0.6$ m, no clear effect is visually apparent. However, the influence becomes quantifiable when considering the standard deviation again. Therefore, weak spots below $d_w = 1.2$ m are not detected numerically as the standard deviation of the CCC value is comparable to that of the homogeneous model.

The results based on model 2-B and model 2-LC-B generally show an increase of the CCC value before the weak spot (see Figure 12(c) and Figure 12(d)). Above the inhomogeneity, the CCC value alternates between decreases and increases. After the weak spot, the initial level is reached again. As the depth d_w increases, the drop in the CCC value above the layer becomes more pronounced and the and the horizontal region influenced by the CCC value expands. From a depth of $d_w = 1.2$ m, the variation of the curves around the homogeneous solution in terms of the standard deviation of the CCC value is roughly of the same order of magnitude.

The decrease in the CCC value due to weak spots, as observed in field measurements (Pistrol and Adam, 2018), was reflected in the simulations based on model 2-A. The other models predict an initial increase in the CCC value when the roller approaches the weak spot, followed by a decrease above it, then an increase in its vicinity. Nevertheless, the oscillatory roller consistently detected the weak spot across all modeling approaches down to a depth of 1.2 m, corresponding to a measurement depth of $d_{CCC} = 1.2$ m.

4 CONCLUSIONS

Numerical investigations were conducted to characterize both the improvement depth d_e of a specific oscillatory roller and the measurement depth d_{CCC} associated with the roller-measured soil stiffness in terms of the compaction indicator for the work-integrated, continuous compaction control (CCC) system for oscillatory rollers developed by Pistrol et al. (2016).

By computing the dynamic drum response of an oscillatory-excited drum on a stationary roller as the thickness of the soft layer increased (elastic layer with $E_L = 16$ MN/m^2 over elastic subsoil with $E_S = 32$ MN/m^2), d_{CCC} was numerically determined to be approximately 0.8 m (with and without driving torque). Although no clear trend in terms of a continuous increase or decrease in the CCC value with layer thickness could be identified, d_{CCC} could nevertheless be derived from the initial decrease followed by an increase to a value varying by approximately ±15% around $CCC^{(d = 5.4\ \mathrm{m})}$ from $d > d_{CCC}$ onwards. Simulations of an oscillatory roller passing over a subsoil with a local heterogeneity (hypoplastic zone with variable depth and $e_0^{(w)}$ values of 0.92 and 0.65, respectively) revealed a measurement depth of $d_{CCC} = 1.2$ m for both the hypoplastic subsoil (Hochstetten sand with $e_0 = 0.56$) and the linear elastic subsoil ($E = 16$ MN/m^2). To investigate the improvement depth, the effect of an oscillatory roller pass on a homogeneous hypoplastic subsoil with initial states ranging from very loose to dense was evaluated in terms of void ratio reduction. Using the Hochstetten sand parameters again, the maximum predicted compaction effect was observed at depths between 0.1 m and 0.4 m, thereby defining the improvement depth d_e. Thus, the numerical simulations consistently predict that d_{CCC} is significantly larger than d_e in all cases.

The ongoing investigations based on the model approaches presented are intended to demonstrate the influence of the following factors on the measurement depth: the stiffness ratio E_L/E_S; the modeling of the layered half-spaces (radially vs. horizontally); the magnitude of the driving torque (approach 1); the more detailed modeling of the roller (with respect to the suspension of the drum) and the modeling of the weak spot (geometry, dimensions, and material behavior, etc.) in model 2; and the amplitude of the tangential drum oscillation.

5 REFERENCES

Adam, D. 1996. *Continuous Compaction Control (CCC) with vibrating rollers* (in German). PhD thesis, TU Wien.

Anderegg, R. and Kaufmann, K. 2004. Intelligent Compaction with Vibratory Rollers: Feedback Control Systems in Automatic Compaction and Compaction Control. *Transportation Research Record* 1868(1), pp. 124-134.

Bergman, R. 2025. *Numerical investigation of the measurement depth during dynamic compaction control with an oscillating roller* (in German). Master's thesis, Universität Innsbruck.

Dassault Systèmes SIMULIA. 2015. Abaqus 2016.

Erdmann, P. and Adam, D. 2014. Numerical simulation of dynamic soil compaction with vibratory compaction equipment. *Proc. XV Danube-European Conf. on Geotech. Eng.*, Vienna, pp. 243-248.

Erdmann, P. 2018. *Numerical simulation of the compaction process in soils with dynamically excited rollers* (in German). PhD thesis, Technische Universität Berlin.

Fathi, A., Tirado, C., Rocha, S. et al. 2021. Assessing depth of influence of intelligent compaction rollers by integrating laboratory testing and field measurements. *Transportation Geotechnics* 28, 100509.

Hager, M. 2022: *CCC with Vibrating Rollers – Development of a new Indicator for Roller-Integrated Continuous Compaction Control* (in German). PhD thesis, TU Wien.

Herle, I. 1997. *Hypoplasticity and particle size analysis of simple soil skeletons* (in German). PhD thesis, Universität Fridericiana Karlsruhe.

Kopf, F. 1999. *Continuous Compaction Control (CCC) during compaction of soil by means of dynamic rollers with different kinds of excitation* (in German). PhD thesis, TU Wien.

Kopf, F. and Erdmann, P. 2005. Numerical investigations of the Continuous Compaction Control (in German). *Österreichische Ingenieur- und Architektenzeitschrift*, 150(4/5), pp. 126-143.

Mašín, D. 2017. *Clay and sand hypoplasticity UMAT and Plaxis implementations, including UMAT-Plaxis interface* [Online]. Available at: https://soilmodels.com [Accessed 25th April 2025].

Niemunis, A. and Herle, I. 1997. Hypoplastic model for cohesionless soils with elastic strain range. *Mechanics of Cohesive-frictional Materials* 2(4), pp. 279-299.

Niemunis, A. 2023. *Incremental Driver 2023* [Online] Available at: https://soilmodels.com [Accessed 2nd April 2025].

Paulmichl, I. 2019. *Numerical modeling approaches to the oscillation roller-subsoil interaction problem*. PhD thesis, Universität Innsbruck.

Paulmichl, I., Adam, C., and Adam, D. 2019. Analytical modeling of the stick-slip motion of an oscillation drum. *Acta Mechanica* 230(9), pp. 3103-3126.

Paulmichl, I., Furtmüller, T., Adam, C. et al. 2020. Numerical simulation of the compaction effect and the dynamic response of an oscillation roller based on a hypoplastic soil model. *Soil Dynamics and Earthquake Engineering* 132, 106057.

Paulmichl, I., Adam, C., and Adam, D. 2020. Parametric study of the compaction effect and the response of an oscillation roller. *Proc. of the Institution of Civil Eng. – Geotech. Eng.* 173, pp. 285-301.

Paulmichl, I., Adam, C., and Adam, D. 2025. Continuous Compaction Control (CCC) for oscillation rollers: development and current investigations (in German). *Bauingenieur* 100(07-08), S. 222-232.

Pistrol, J. 2016. *Compaction with oscillating rollers. Motion behaviour, roller integrated compaction control and assessment of wear* (in German). PhD thesis, TU Wien.

Pistrol, J., Villwock, S., Völkel W, et al. 2016. Continuous Compaction Control (CCC) with oscillating rollers. *Procedia Engineering* 143, pp. 514–521.

Pistrol, J. and Adam, D. 2018. Fundamentals of roller integrated compaction control for oscillatory rollers and comparison with conventional testing methods. *Transportation Geotechnics* 17, Part B, pp. 75-84.

Rinehart, R.V. and Mooney, M.A. 2009. Measurement depth of vibratory roller-measured soil stiffness. *Géotechnique* 59(7), pp. 609-619.

Wolf, T. 2022. *UMAT implementation of a hypoplastic constitutive law for numerical simulation of dynamic soil compaction* (in German). Master's thesis, Universität Innsbruck.

von Wolffersdorff, P.A. 1996. A hypoplastic relation for granular materials with a pre- defined limit state surface. *Mechanics of Cohesive-frictional Materials* 1(3), pp. 251–271.